ORIGINAL ARTICLE

Considering multiple process observables to determine material model parameters for FE-cutting simulations

Marvin Hardt[1] · Thomas Bergs[1,2]

Abstract

Analyzing the chip formation process by means of the finite element method (FEM) is an established procedure to understand the cutting process. For a realistic simulation, different input models are required, among which the material model is crucial. To determine the underlying material model parameters, inverse methods have found an increasing acceptance within the last decade. The calculated model parameters exhibit good validity within the domain of investigation, but suffer from their non-uniqueness. To overcome the drawback of the non-uniqueness, the literature suggests either to enlarge the domain of experimental investigations or to use more process observables as validation parameters. This paper presents a novel approach merging both suggestions: a fully automatized procedure in conjunction with the use of multiple process observables is utilized to investigate the non-uniqueness of material model parameters for the domain of cutting simulations. The underlying approach is two-fold: Firstly, the accuracy of the evaluated process observables from FE simulations is enhanced by establishing an automatized routine. Secondly, the number of process observables that are considered in the inverse approach is increased. For this purpose, the cutting force, cutting normal force, chip temperature, chip thickness, and chip radius are taken into account. It was shown that multiple parameter sets of the material model can result in almost identical simulation results in terms of the simulated process observables and the local material loads.

Keywords Inverse identification · Machining model parameters · Downhill simplex algorithm · Johnson-Cook model · Cutting simulation

1 Introduction

The use of simulation techniques, such as the finite element method (FEM), to model the machining process enables the prediction of difficult-to-measure process quantities, such as stresses, strains, and temperature fields [1, 2]. The knowledge about these quantities plays a pivotal role to improve the process understanding and the identification of the acting mechanisms. Machining simulations offer the possibility to enhance the process design by overcoming classical, empirical "trial-and-error" approaches [3, 4]. In metal cutting, the backbone of such a simulation is the chip formation process. To model the chip formation process by means of FE simulations, different parameters and input models are required. Among them, the material and friction models are essential for the reliability and accuracy of simulated results [5–7].

In the state of the art, the determination of material model parameters is conducted by two different approaches:

- By direct determination of the model parameters from conventional tests (e.g., tensile tests) and non-conventional material tests (e.g., split Hopkinson pressure bar (SHPB) tests), or
- By inverse techniques.

For direct tests, the thermo-mechanical loads are limited, wherefore the occurring loads are far away from those of the cutting process [4, 8] and extrapolation into the regime of metal cutting becomes necessary [9–12]. This extrapolation into the regime of metal cutting conditions can cause inaccuracies of the

✉ Marvin Hardt
  m.hardt@wzl.rwth-aachen.de

1 Laboratory for Machine Tools and Production Engineering (WZL) of RWTH Aachen University, Campus-Boulevard 30, 52074 Aachen, Germany

2 Fraunhofer Institute for Production Technology IPT, Steinbachstr. 17, 52074 Aachen, Germany

simulated results [13]. To overcome this issue, Venuvinod and Jin suggested to use the cutting process itself as a material test [14], since a process can be represented best by itself in terms of the occurring loads. For this inverse parameter determination, the model parameters are iteratively modified until the simulations of the process are in agreement with the experimental measurements. Therefore, different process observables are assessed to evaluate the deviation between simulations and experiments, such as the process forces or the chip form.

The inverse parameter determination has found increased application within the last decade. Özel and Altan presented one of the first approaches for the inverse parameter determination from the cutting process [15]. To calibrate the material model parameters for AISI P20 mold steel, flow stress data from strain and strain rate tests were used as starting point to model the chip formation process, followed by an iterative fitting of the parameters. To evaluate the match between experimental and simulative data, only the cutting force was considered. However, Bäker reported that it is not sufficient to consider just the cutting force, since the cutting force is less sensitive to an accurate material model than other integral process observables [16]. Further studies on the inverse parameter determination for metal cutting simulations were presented by Shrot and Bäker [17–20]. The authors developed a procedure that bases on the Levenberg-Marquardt algorithm, which was utilized for the inverse determination of the Johnson-Cook (JC) material model parameters A and B. Their results showed that it was possible to re-identify the material model parameters within a relatively small number of iterations. However, it remains uncertain if the procedure is applicable for the inverse determination of all JC material model parameters. Klocke et al. presented a method for the inverse parameter determination of the JC parameters C and m [21, 22]. Therefore, lower and upper values of the parameters were guessed and their results were interpolated in order to find the best fit with the experimental results. Later, Klocke et al. presented a pure iterative procedure for the inverse determination of material and friction parameters of Inconel 718 Direct Aged [23]. Albeit, their procedure is dependent on the experience of the user, wherefore the robustness remains questionable. Zhang et al. developed a novel procedure for the inverse determination by taking cutting forces and deformation fields into account, which were measured by means of the digital image correlation (DIC) [24]. Due to technical limitation of the utilized DIC system, only low cutting speeds of up to $v_c \leq 0.1$ mm/min were considered. Further, the effect of strain rate hardening and thermal softening was neglected, which are two important effects that influence the material behavior in the cutting process. Besides the outlined drawbacks of the inverse parameter determination, Arrazola et al. [3] and Shrot and Bäker [25] reported that an absolute solution of the parameter set in not necessarily given, because many combinations of parameters can result for the investigated

domain in the same simulation results, which means that the material model parameters are not unique [2].

To reduce the computational effort and to increase the robustness of the solution, optimization algorithms were applied to the inverse problem. In the field of sheet metal forming, Chaparro et al. utilized a genetic and a gradient-based algorithm for the inverse determination of material model parameters [26]. The authors showed that it was possible to fit the numerical with experimental data by using optimization algorithms. For machining simulations, Özel and Karpat used the Particle Swarm Optimization to determine JC parameters [27]. As experimental data basis, the authors utilized SHPB tests, which required extrapolation into the domain of metal cutting.

To improve the inverse parameter determination, the authors of this paper developed a novel approach by using the Downhill simplex algorithm (DSA). In previous papers, this optimization algorithm was examined regarding its potentials for the inverse problem [28], its applicability for experimental results [29], and its influencing factors [30]. However, the results of these studies resulted in non-unique parameter sets for the domain of investigation. Further, the evaluation of the simulations required a manual comparison between the simulations and the experimentally derived chip form, which was characterized by high efforts and limited accuracies [30]. Different approaches for this inverse re-identification were used, all suggesting that the parameters sets are not unique. However, the simulated process observables deviated just slightly. For the developed procedure, two drawbacks were eminent: the effort to evaluate the simulations and the accuracy of the manually determined simulation results. For the iterative procedure, the effort to evaluate the chip formation simulations can easily sum up to multiple days. When analyzing the results from FE simulations, the determined results and their accuracy depend on simulation-inherent parameters, such as the mesh size as well as on the user, who analyzes the simulations. Some relevant simulation results that can be used for the comparison between simulations and experiment can only be extracted with high efforts, such as the chip radius.

The novelty of this paper is two-fold: in the first part, an approach for an automated inverse determination of material model parameters from coupled Eulerian-Lagrangian (CEL) FE chip formation simulations is developed. Further, the number of process observables to assess the deviations between experiments and simulations is increased. To extract information on the chip form from CEL simulations, a method to reconstruct the chip contour was developed and validated.

In the second part, the automated evaluation of chip formation simulations is employed in an optimization-based inverse parameter determination. The non-uniqueness is evaluated in terms of the considered process observables as well as the local thermo-mechanical material loads.

The paper is organized as follows: in the following chapter, the CEL model of orthogonal cutting is presented. Thereafter,

the theoretical background of the two-fluid interface problem is outlined and applied to orthogonal cutting simulations. Further, a methodology to extract process observables from the FE simulations is developed. The automatized analysis is integrated in an inverse parameter determination procedure. Inverse re-identification approaches are conducted and the calculated parameter sets are evaluated. Thereafter, the results are discussed. At the end of the paper, a summary will be given and an outlook will be drawn.

2 Coupled Eulerian-Lagrangian model of orthogonal cutting

To model the chip formation process, a CEL model of orthogonal cutting was developed within the commercial simulation software Abaqus 6.14-6. Orthogonal cutting was chosen as cutting process since it can be considered as the most elementary process and allows to consider the process as two-dimensional. The CEL formulation was firstly applied by Klocke et al. [31] and Ducobu et al. [32] to the field of machining. In the CEL model, the tool was discretized by using the Lagrangian formulation. For the Lagrangian tool, 8-node thermally coupled elements of type C3D8RT were utilized. The workpiece material on the other side was modeled by the Eulerian formulation so that the material can freely flow through the mesh. Therefore, 8-node thermally coupled linear Eulerian elements with reduced integration and hourglass control (C3D8RT) were used. Additionally, an area for the formation of the chip and an area of the machined material were discretized by the Eulerian formulation. Thereby, the chip was not restricted in its form, but only in its length, which in turn was limited by the size of the modeled domain. Within the Eulerian and the Lagrangian domain, the minimal mesh size

was 5 μm. For the simulations, the explicit formulation was utilized, which is favorable for non-linear dynamic problems such as the metal cutting process [3]. The setup of the CEL model that was used is illustrated in Fig. 1. It resembles a model used in a previous study by the authors [28].

An initial inflow of the material was used to model the cutting speed v_c. The inflowing material exited the Euler domain either in form of the chip or as machined material. For all conducted simulations, a cutting length of $l_c = 3.33$ mm was utilized. This cutting length showed to be sufficient to reach the steady state in the simulations. To reduce the computational time of the simulations, a mass scaling factor of 1000 was applied. The simulations were conducted on a virtual machine with 16 CPU of type Intel® Xeon® CPU E5-2698v4 with 2.2 GHz. For each simulation, 4 CPU were used. Therefore, a simulated cutting time of $t_c = 0.002$ s required approximately 2 h and 20 min of computational time. Further details on the used material parameters, material properties, and boundary conditions are given in [28].

The JC material model was utilized to model the material behavior of AISI 1045 [33]. The JC model is one of the most widely used material models to describe the constitutive workpiece material behavior in metal cutting simulations, Eq. (1). AISI 1045 was chosen as material of investigation, since this material tends to form a continuous chip over a wide range of cutting conditions. Therefore, a damage model to simulate chip segmentation was not considered within this study.

$$\sigma_{fl} = (A + B \cdot \epsilon^n) \cdot \left(1 + C \cdot ln\left(\frac{\dot{\epsilon}}{\dot{\epsilon_0}}\right)\right) \cdot \left(1 - \left(\frac{T - T_0}{T_m - T_0}\right)^m\right) \quad (1)$$

In the JC model, the effects of strain hardening, strain rate hardening, and thermal softening are considered by the three separate terms in the brackets. The variables A, B, C, n, and m are the model parameters, which are assumed to be constant,

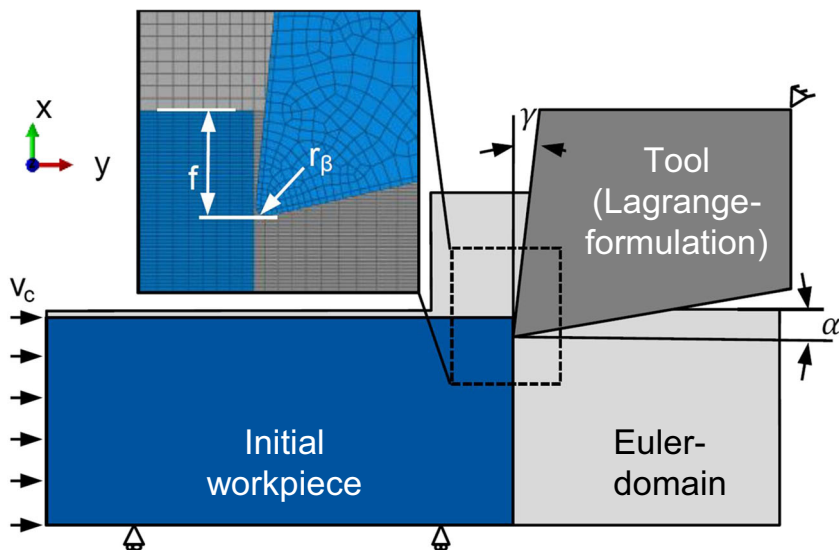**Fig. 1** Setup of the coupled Eulerian-Lagrangian FE model of orthogonal cutting [28].

Table 1 Johnson-Cook material model parameters for AISI 1045 [29]

A / MPa	B / MPa	n / –	m / –	C / –	$\dot{\epsilon}_0$ / s^{-1}	T_0 / °C	T_m / °C
546	487	0.25	0.631	0.027	0.002	20	1500

T_m is the material's melting temperature, and the symbols $\dot{\epsilon}_0$ and T_0 denote reference values. In the present paper it is aimed to evaluate the developed methodology for the inverse parameter determination. Therefore, the routine is applied to the inverse re-identification of material model parameters. The material model parameters to be inversely re-identified were taken from the literature [22] since they are unknown a priori when using experimental data (Table 1). This allows an evaluation of the determined parameter sets in comparison to the target parameter set and, therefore, an assessment regarding the uniqueness of material model parameters. Since numerical errors, such as rounding errors, can occur in FE simulations, non-uniqueness is assumed in this paper if the evaluated results differ by less than 1%.

3 Two-fluid interface problem

The determination of the chip form from CEL simulations is a two-phase problem, where the interface of the two phases needs to be determined. In order to calculate the chip form, established methods from the field of fluid mechanics are transferred to the given task. In CEL cutting simulations, the two-phase flow is given by material that flows in the void of the Euler domain. The method aims to decrease the evaluation time and to increase the accuracy of the results. Simplified, the problem of two immiscible fluids in a mesh can be sketched in a fixed coordinate system, where some cells are fully filled with one fluid (Fig. 2a, blue region) and others with a different fluid (Fig. 2a, gray region). The cells filled with both fluids define the two-fluid interface. The volume-of-fluid (VOF) method is a widespread technique to analyze interfaces in
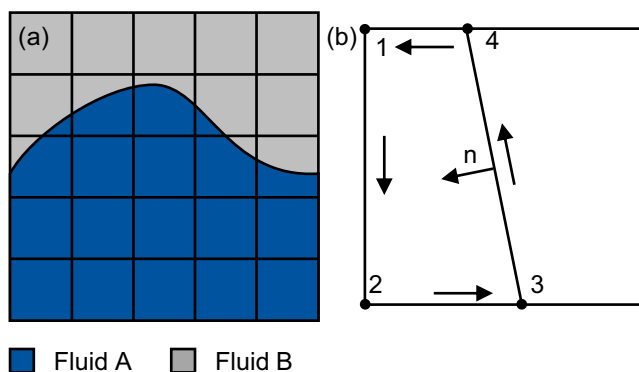
Fig. 2 **a** Sketch of a two-fluid configuration. **b** Four-sided polygon form when an interface line truncates a cell

■ Fluid A　　■ Fluid B

two-phase flows [34]. Within this study, the concept of the VOF is applied to determine the chip form.

For the reconstruction of the two-fluid interface, volume-tracking methods were applied, which differ by the features of the interface reconstruction algorithm and by the time integration of the volume fraction advection equation. Rider and Kothe [35] proposed a piecewise linear interface calculation (PLIC) method and a multi-dimensional unsplit time integration scheme, in which material volume fluxes are computed by using a set of simple geometrical tasks.

Within the CEL simulation in Abaqus, the concept of the Eulerian volume fraction (EVF) is used to describe the fraction volume of a cell occupied by a fluid. In this concept, the EVF is equal to one in the case that the cell is filled with the fluid and zero if the cell does not contain the fluid or a different fluid. Cells that contain a portion of the fluid in its volume have an EVF proportional to the share of the fluid and are called mixed cells. For these cells, the border between the two fluids can be approximated by polygons. This can be done with the piecewise linear interface calculation (PLIC) [35]. The algorithm bases on a second-order geometric solution of a volume evolution equation. The method uses local discrete material volume and velocity data to track the surface of a topology. In a single cell of a two-dimensional regime, the geometric function for the interface is assumed to be a straight line. For the application to CEL-chip formation simulations, the assumption of a straight line instead of a function of higher order appeared to be reasonable, as long as the mesh size is small. The assumption of the straight line will be evaluated in section 4.1.

Afterwards, the resulting polygon can be defined. The vertices of the polygon of a mixed cell (x_v, y_v) are those lying inside the fluid (points 1 and 2) and the intersection points of the cell and the straight line (points 3 and 4) (Fig. 2b). The n-sided polygon in a Cartesian x/y-geometry surrounds the fluid in each cell, whereby the matrix of the enclosed area A is calculated according to:

$$A = \frac{1}{2} \cdot \sum_{v=1}^{n} \left(x_v \cdot y_{v+1} - x_{v+1} \cdot y_v \right). \tag{2}$$

Based on the given equations, the linear interface has to be reconstructed for every mixed cell of the mesh. The line constant ρ can be calculated by volume conservation, and the normal n is calculated from volume fraction gradients. The value of ρ is limited in such a way that the volume of the polygon is equal to the volume of the fluid within the cell. This relationship can be described in the 2D case by:

$$\frac{A_\rho}{A_c} - EVF = 0, \tag{3}$$

where A_c is the total cell area and A_ρ the area of the polygon.

An established method to calculate the normal vector for general meshes is the extension of Youngs' second method

[36] that was developed by Kothe et al. [37]. In the algorithm, the finite-difference approximations to determine the volume fraction gradient ∇f are utilized. This procedure is derived from the work of Barth [38], who developed the linear and quadratic reconstruction of discrete data on unstructured meshes based on least square algorithms. For this approach, volume fraction Taylor series expansions f_i^{TS} are formed from each reference cell volume fraction f_i at x_i to each neighbor cell f_k at x_k. The sum $\left(f_i^{TS}-f_k\right)^2$ over all n direct neighbors is minimized. The result is the volume fraction gradient ∇f_i, Eq. (4) to Eq. (10).

$$A^T A\, x = A^T b \tag{4}$$

where

$$A = \begin{pmatrix} \omega_k(x_k-x_i) & \omega_k(y_k-y_i) \\ \vdots & \vdots \\ \omega_n(x_n-x_i) & \omega_n(x_n-x_i) \end{pmatrix} \tag{5}$$

$$b = \begin{pmatrix} \omega_k(f_k-f_i) \\ \vdots \\ \omega_n(f_n-f_i) \end{pmatrix} \tag{6}$$

$$\omega_k = \frac{1}{|x_k-x_i|^2} \tag{7}$$

$$X = \begin{pmatrix} \nabla_x f_i \\ \nabla_y f_i \end{pmatrix} \tag{8}$$

The normal vector is computed as:

$$n = \begin{pmatrix} \dfrac{\nabla_x f_i}{|\nabla f_i|} \\ \dfrac{\nabla_y f_i}{|\nabla f_i|} \end{pmatrix}, \tag{9}$$

where

$$|\nabla f_i| = \sqrt{(\nabla_x f_i)^2 + (\nabla_y f_i)^2} \tag{10}$$

4 Reconstruction of the chip geometry from CEL-cutting simulations

The EVF values and the position of the elements are extracted from the simulations to apply the theory of the two-fluid interface problem and to reconstruct the chip form. The centroid position of the elements was calculated in the region of the CEL model, where the chip forms and only those elements with $0 < \text{EVF} < 1$ were considered. To determine the normal vector n of each mixed-cell element, the PLIC method in conjunction with Youngs' least square method was utilized. Thereby, the results from each cell were linked with the results from its neighbor cells.

The information on the EVF values, total element area, and normal vectors were used to iteratively solve Eq. (3). For the iterative procedure, the Wijgaarden-Dekker-Brent method [39], also known as Brent's method, was used. Brent's method combines parts of the bisection method, secant method, and inverse quadratic interpolation. The advantage of using Brent's method is that the algorithm converges for functions computable within a fixed interval [40]. Here, the interval is defined by the lower and upper boundaries ρ_{min}, ρ_{max}. These boundaries are estimated based on the position of the cell vertices and their normal direction (Fig. 3). As convergence criterion, a remaining error in Eq. (3) of 0.01 % was defined.

After the algorithm runs through all of the mixed cells, the geometry of the chip can be reconstructed (Fig. 4).

4.1 Determination of chip form parameters

To determine the chip form parameters, the simulated length must be limited in such a way that the chip does not hit the surface of the workpiece and curls up. This would affect the chip radius. The two chip form parameters that are evaluated within this study are the chip thickness h and the chip radius r_c. The reconstruction provides the circumference of the chip with an outer radius r_{out} at the tool side and an inner radius r_{in} at the free chip surface. The calculation neglects a certain distance in the x-direction within the Euler domain to avoid the influence of the chip curl. Based on the calculation of the centroid coordinates, the value of the chip radius can be determined using the equation of a circle. The results of the calculated radii are averaged in the inner and outer chip radius r_c. A least squares approach is employed to calculate the centroid of the circumferences. The generalized matrix to compute the coordinates of the chip centroid (O_x, O_y) is given in Eq. (11), where P_i are the determined points on the outer circumference of the chip.

$$\begin{bmatrix} P_{1_x}-P_{2_x} & P_{1_y}-P_{2_y} \\ \vdots & \vdots \\ P_{n-1_x}-P_{n_x} & P_{n-1_y}-P_{n_y} \end{bmatrix} \begin{bmatrix} O_x \\ O_y \end{bmatrix} = \frac{1}{2} \begin{bmatrix} P_{1_x}^2-P_{2_x}^2 + P_{1_y}^2-P_{2_y}^2 \\ \vdots \\ P_{n-1_x}^2-P_{n_x}^2 + P_{n-1_y}^2-P_{n_y}^2 \end{bmatrix} \tag{11}$$

Using the least squares approach leads to a numerical residue, which is also given to evaluate the results. The numerical
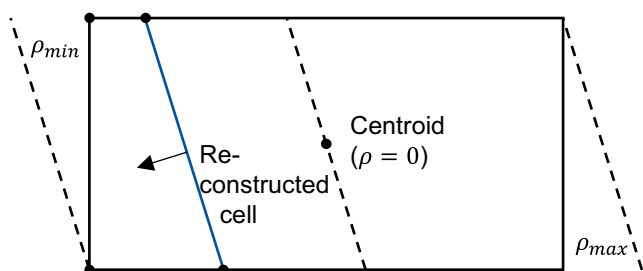

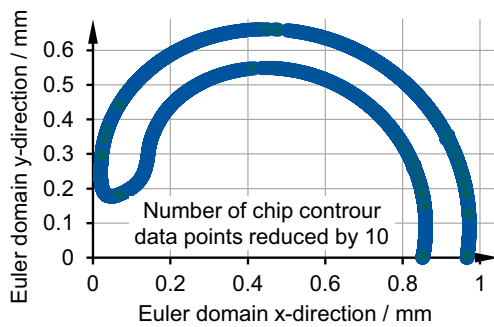**Fig. 3** Schematic representation of the entities in the cell reconstruction routine

Fig. 4 Example of the reconstructed chip geometry

Fig. 5 Comparison of the automatically and the manually determined chip thicknesses from FE chip formation simulations

residue describes the deviation of the numerical determined results from a perfect fit.

Finally, the chip thickness h' is calculated as the difference between the outer and the inner chip radius, Eq. (12).

$$h' = r_{out} - r_{in} \tag{12}$$

4.2 Validation and evaluation of the determined chip form parameters

To evaluate the automatized determination of the chip form parameters from FE chip formation simulations, the results from the algorithm were compared with the manual measured ones from the simulated chip form and to each other by the resulting residue. The chip radius was not considered, since it is impossible to measure it accurately by hand.

When using the automated approach, the residue was in every case lower than $R_{max} < 5 \times 10^{-5}$ mm. This is smaller than the smallest mesh size within the Euler domain ($l_{mesh,min}$ = 0.005 mm). This suggests a reasonable good agreement with the underlying data points. It also confirms that linear elements are sufficient to reconstruct the borderline.

The comparison of the manually and the automatically determined chip thicknesses is shown in Fig. 5 for different cutting speeds and undeformed chip thicknesses. The results emphasize that the values of the automatic procedure and of their manually determined counterparts are in a close agreement. This can be attributed to the small mesh size enabling a high resolution of the chip contour. However, the standard deviations of the manual measurements were higher.

5 Extraction of process observables from FE-chip formation simulations

Besides the chip form, other process observables, such as the cutting force, cutting normal force, or thermal measurements, were used to validate cutting simulations. When evaluating the cutting force components from cutting simulations, the forces are usually averaged within the region of steady state.
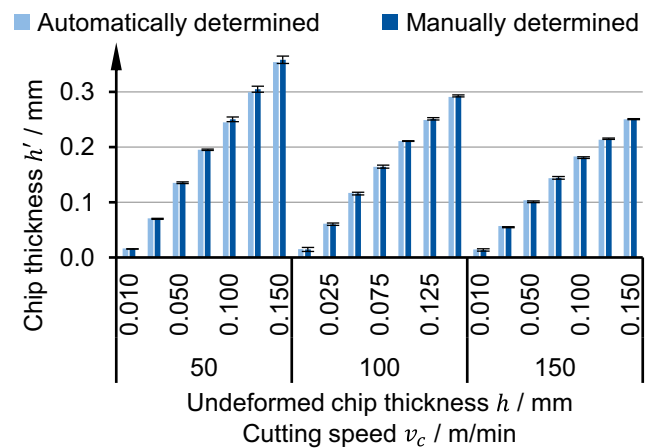
To have single values representing the mechanical reaction forces in each coordinate direction and to establish a consistent procedure to evaluate the force signals, a data filter was applied to the automatized evaluation of FE chip formation simulations. The filter function bases on the temporal averages and its differences [41]. Therefore, the simulated signals of the cutting force and cutting normal force are firstly passed through a Wiener filter to reduce undesired noise and eliminate outliers that would cumber the definition of equilibrium [42]. Afterwards, a moving average with a step size of 5% of the total signal length is applied. The resulting list of averages is tested for the minimal discrepancy to its neighbors. If the resulting discrepancy is lower than the tolerated one, which was set to 5%, the function is considered to be in the steady state. Additionally, the end of the signal is cut off, since it can include undesired residues. An example of the force evolution is shown in Fig. 6.

As a further process observable, the chip temperature was taken into account in the inverse re-determination, since it was possible to measure the chip temperature experimentally [29]. For the proper evaluation of the chip temperature, the measuring position as well as the diameter of the measuring spot was taken into account (Fig. 7). The tool-sided chip temperature was averaged within a spot of 25 μm diameter.
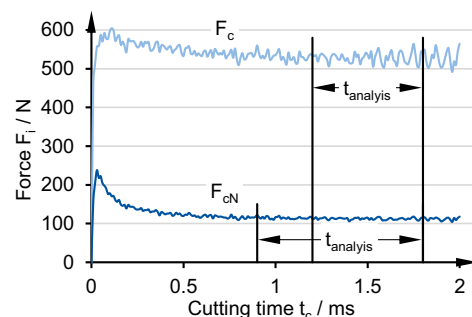

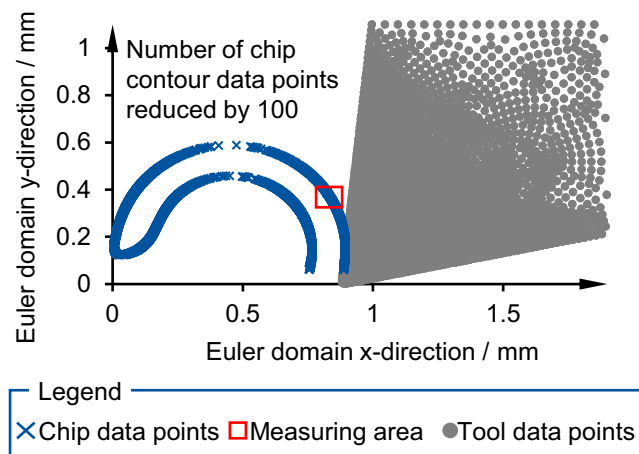**Fig. 6** Regime of the steady-state cutting force and cutting normal force

Fig. 7 Determination of the tool-sided chip temperature within a predefined area

6 Downhill simplex algorithm for inverse material model parameter determination

The developed procedure to analyze the results from FE chip formation simulations was utilized in an inverse determination of material model parameters. Therefore, an initial parameter set from the literature was used [22] (Table 1). With this parameter set, the chip formation process was simulated and the process observables were extracted from the simulations as target values for the inverse parameter determination.

To evaluate the deviation between the iterative simulation results x_{sim} and the target values x_{target} of the considered process observables, the observables are weighted in a single objective function:

$$\xi = \sum_i^n \omega_i \cdot \left| \frac{x_{target} - x_{sim}}{x_{target}} \right|, \tag{13}$$

where ω_i are weighting factors that weight the individual process observables. Their values were set based on established empirical values to $\omega_{F_c} = 0.30$, $\omega_{F_{cN}} = 0.15$, $\omega_{h'} = 0.20$, $\omega_{r_c} = 0.20$, and $\omega_T = 0.15$.

The optimization was performed with the Downhill simplex algorithm (DSA) [28–30]. The DSA, also known as Nelder-Mead simplex algorithm [43], is an unconstrained direct search method for multi-dimensional optimization [44]. For the optimization in an n-dimensional search space, the algorithm compares $n + 1$ vertices and replaces the worst vertex in terms of the evaluation function ξ. Five different operators are applied within the algorithm that modify the simplex spanned by the vertices. The operators are reflection, expansion, internal and external contraction, and shrinkage. The parameters of the operators that influence the step size of the algorithm were set to $\rho_{DSA} = 1$ (reflection), $\epsilon_{DSA} = 0.5$ (expansion), $\kappa_{DSA} = 0.5$ (internal and external contraction), and $\sigma_{DSA} = 0.5$ (shrinkage) [28, 30].

The initial simplex for the conduction of the algorithm was randomly generated and the boundaries of the to-be-determined JC parameters were limited to physical meaningful ranges (Table 2). The same initial simplexes were used as in [30] to study if multiple process observables lead to a reproducible (i.e., "unique") identification of material model parameters for the domain of investigation.

Three conditions were defined as termination criteria for the optimization:

(i) Error criterion: the error value, Eq. (13), undercuts a value of $\xi \leq 1\%$ for all cutting conditions.
(ii) Convergence criterion I: the individual parameters of two consecutive sets deviate by less than 1%.
(iii) Convergence criterion II: the improvement in the error function value is less than $\Delta\xi \leq 0.1\%$ for two consecutive iterations.

The initial JC parameter set ("target parameter set") was used to simulate the orthogonal cutting process for different cutting conditions (Table 3). Multiple cutting conditions were used for the inverse re-identification since it was expected to enhance the reliability of the model parameters due to the increased domain of investigation and the increased spectrum of occurring thermo-mechanical loads [16, 20, 25].

Table 2 Underlying parameter sets used for the initial simplexes of the Downhill simplex algorithm

	Vertex	A / MPa	B / MPa	n / −	m / −	C / −
Initial simplex 1	1	350	400	0.150	0.150	0.017
	2	700	550	0.350	0.750	0.040
	3	400	525	0.330	0.550	0.150
	4	435	420	0.500	0.400	0.035
	5	625	375	0.175	0.800	0.020
	6	490	415	0.700	0.330	0.100
Initial simplex 2	1	328	409	0.648	0.258	0.116
	2	548	544	0.283	0.359	0.010
	3	514	605	0.164	0.556	0.063
	4	344	558	0.211	0.105	0.112
	5	493	667	0.770	0.400	0.140
	6	689	711	0.501	0.844	0.067
Initial simplex 3	1	409	519	0.582	0.103	0.091
	2	505	648	0.544	0.766	0.120
	3	500	679	0.866	0.648	0.084
	4	661	585	0.664	0.286	0.057
	5	427	608	0.449	0.404	0.019
	6	312	658	0.869	0.528	0.014
Upper bound		300	350	0.100	0.100	0.005
Lower bound		700	750	0.900	0.850	0.150

Table 3 Cutting conditions for the inverse parameter re-identification

Cutting speed v_c / m/min	50	100	150
Undeformed chip thickness h / mm	0.05		

Figure 8 shows the results of the DSA starting with simplex 1, where the resulting error values ξ for the three cutting conditions are plotted over the iterations N. The diagram shows an exponentially decreasing error value. The optimization terminated after 82 iterations due to convergence criterion I (less than 1 % change in the parameters for consecutive iterations). For the conducted approach, the lowest error values were obtained at iteration 43, wherefore the average error value for the three cutting conditions was $\xi_{aver} = 1.1\%$. The error values of the individual cutting conditions were $\xi_{50} = 1.66\%$, $\xi_{100} = 0.98\%$, and $\xi_{150} = 0.80\%$. Besides the good fit, the obtained parameters deviated distinctively from the target parameters. For the domain of investigation, this does not support the hypothesis of a unique material model parameter set nor that using multiple cutting conditions foster unique parameter sets.

Analyzing the evolution of the error values reveals that the algorithm gets stuck in a local minimum. The global minimum is given by the target parameter set. The determination of a local minimum can mainly be attributed to two influencing factors: to the DSA, which is a local optimization algorithm, and to the existence of multiple local minima.

For the initial simplex 2, the results are shown in Fig. 9. It shows lower error values from the beginning. It seems that this set of random parameters better describes the three different cutting conditions. The approach was terminated after 92 iterations, due to convergence criterion II. The lowest error values were calculated for iteration 80, with an average error value of $\xi_{aver} = 1.6\%$. The individual error values of the three
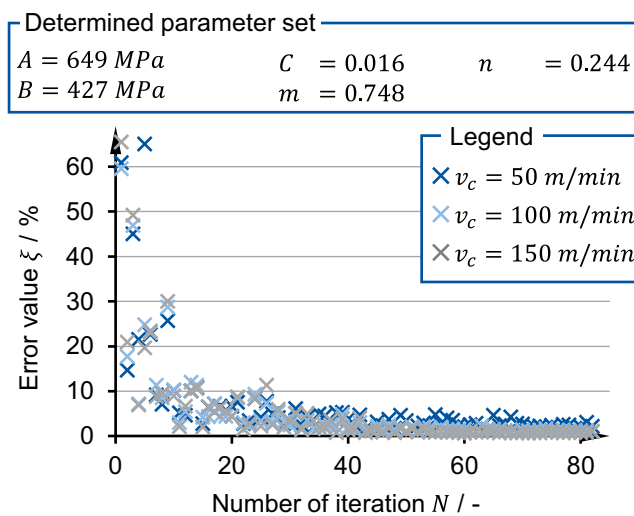
Determined parameter set

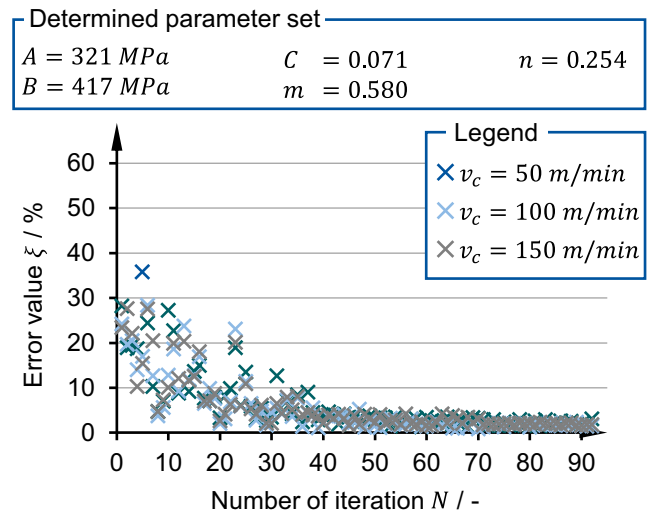| $A = 321\ MPa$	$C = 0.071$	$n = 0.254$
$B = 417\ MPa$	$m = 0.580$	

Fig. 9 Development of the error value for the investigated cutting conditions using the initial simplex 2

investigated cutting condition were $\xi_{50} = 1.43\%$, $\xi_{100} = 1.23\%$, and $\xi_{150} = 2.12\%$.

Again, the target parameter set was not obtained. By using two different initial simplexes, two different parameter sets were determined, which both produced low error values.

Figure 10 provides the evolution of the DSA for the initial simplex 3. The inverse identification was terminated after 92 iterations, due to the second termination criteria (convergence criterion I). In this case, the lowest parameter set was determined by iteration 91. For the calculated parameter set, the average error value was $\xi_{aver} = 0.99\%$. The error values of the underlying cutting conditions were $\xi_{50} = 1.11\%$, $\xi_{100} = 0.66\%$, and $\xi_{150} = 1.18\%$.

The parameter set deviated from the target parameter set as well as from the determined parameter sets of the other two
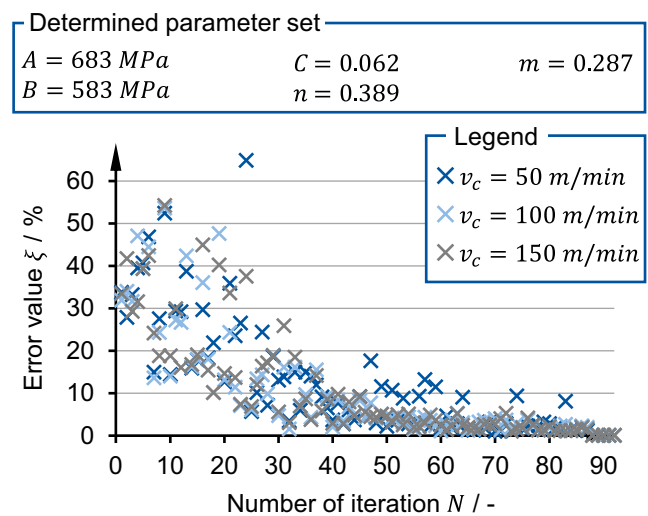
Determined parameter set

$A = 649\ MPa$	$C = 0.016$	$n = 0.244$
$B = 427\ MPa$	$m = 0.748$	

Fig. 8 Development of the error value for the investigated cutting conditions using the initial simplex 1

Determined parameter set

$A = 683\ MPa$	$C = 0.062$	$m = 0.287$
$B = 583\ MPa$	$n = 0.389$	

Fig. 10 Development of the error value for the investigated cutting conditions using the initial simplex 3

approaches. For the domain of investigation, the non-uniqueness of the JC material model parameters results in multiple local minima.

7 Discussion

In the iterative procedure of this study, the deviation of a process observable from its target value was assessed by means of the merged error value ξ, Eq. (13). To evaluate the accuracy of the developed method, the relative errors of the individual process observables in comparison to their target values are given in Table 4 for the cutting condition $v_c = 100$ m/min, and $h = 0.05$ mm. The highest deviations occurred in parameter set 3, wherefore the cutting normal force deviated by 1.2% from its target value. Numerical inaccuracies can only be held accustomed for minor differences in the order of a tenth of a percent. The chip form parameter showed the largest deviations. The chip radius deviated at most by 3.8% from its target value. The approaches revealed that the chip radius r_c is very sensitive to the material model parameters. Even slight changes in the material model parameters have a significant effect on the chip radius.

The investigations suggested that the model parameter sets were not unique—at least in the considered domain of cutting conditions and for the considered process observables. In all cases, the error value was smaller than 2% suggesting the existence of multiple suitable local minima. To assess the accuracy of the determined parameter sets, the calculated material model parameters and the target parameter set are summarized in Table 5. The largest deviations occurred in the material model parameters A, C, and m. For these parameters, the differences can be larger than 100%. This results in a drastically different material behavior—respectively flow stress—with regard to the thermo-mechanical loads. There are multiple parameter sets, which may serve equally good to model the material behavior for the specific loads for the investigated domain.

Figure 11 shows the resulting flow stresses separately listing the three influences on the flow stress that are considered

Table 4 Relative deviations of the process observables in comparison to their target values

	Set 1	Set 2	Set 3
Rel. cutting force F_c / %	99.0	100.1	100.0
Rel. cutting normal force F_{cN} / %	100.5	99.9	101.2
Rel. chip thickness h / %	101.3	97.8	97.6
Rel. chip radius r_c / %	98.4	96.2	101.9
Rel. chip temperature T / %	99.5	100.9	100.8

Cutting condition: $v_c = 100$ m/min, $h = 0.05$ mm

Table 5 Determined parameter sets for the conducted approaches

	A / MPa	B / MPa	C / $-$	n / $-$	m / $-$
Target set	546	487	0.027	0.250	0.631
Set 1	649	427	0.016	0.244	0.748
Set 2	321	417	0.071	0.254	0.580
Set 3	683	583	0.062	0.389	0.289

by the JC model (strain hardening, strain rate hardening, and thermal softening). In the first term of the JC material model, the flow stress is calculated for different strains, whereas the
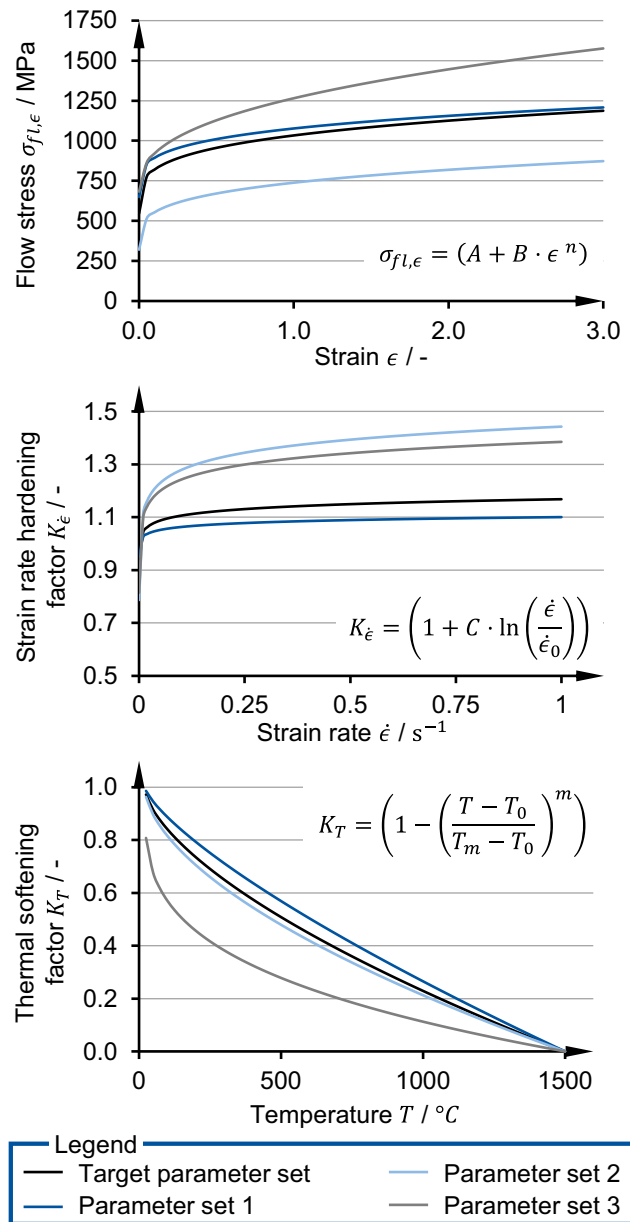

Fig. 11 Comparison of the material behavior for the three different terms of the Johnson-Cook material model representing the strain hardening, strain rate hardening, and thermal softening for the target parameter set and the determined parameter sets

effect of strain rate hardening and thermal softening is considered by a hardening factor $K_{\dot\epsilon}$ and a softening factor K_T. The curves show that for the identified parameter sets, the effect of strain hardening, strain rate hardening, and thermal softening are modeled differently. Among the three determined parameter sets, parameter set 2 resulted in the lowest flow stress for increasing strains. This is mainly attributed to the low value of parameter A, which defines the initial flow stress. On the contrary, parameter set 2 resulted in the highest strain rate hardening factor, since parameter C was higher than for the other parameter sets. Parameter set 3 on the other side resulted in the highest flow stress for increasing strains and in the lowest thermal softening factor K_T.

The differences in the magnitudes emphasize that the three effects can compensate each other within the investigated regime of machining conditions. Thereby, increased strain or strain rate hardening can be compensated by a higher thermal softening effect and vice versa. This observation can be considered as a drawback of the JC model for machining simulations, due to its uncoupled nature [45]. Material models with a coupled term, which takes the mutual influence of the effects into account, could solve this drawback. However, the reciprocal compensation of the three effects is expected to be reduced by considering experimental results from different domains, such as from quasi-static, dynamic material tests (e.g., SHPB tests), and cutting tests. From conventional material tests, different parameters can be determined directly by means of a curve fitting routine. This procedure would further reduce the number of parameters to be inversely calculated.

The inverse determination based on the minimization of the error value function ξ, Eq. (13). To compare the simulated results of the determined parameter sets regarding the occurring loads, Fig. 12, Fig. 13, and Fig. 14 show the results of the chip formation simulations for the same cutting conditions. Figure 12 shows the results regarding the local temperature field, Fig. 13 the plastic strains, and Fig. 14 the equivalent stresses. The comparison of simulated local temperatures, Fig. 12, revealed small deviations in terms of the absolute temperature and the expansion of the temperature fields for the different material model parameter sets. Thereby, the deviations between parameter set 1 and the target parameter set as well as between parameter set 2 and parameter set 3 were almost not identifiable. In comparison with the temperature field of the target parameter set, parameter set 2 and parameter set 3 resulted in a spatially more pronounced temperature profile.

The simulated chip form tended to deviate between the approaches, especially at the beginning of the chip formation. This is due to the individual differences regarding the three considered hardening and softening effects within the non-steady state of the machining process. The differences of the chip form became smaller for longer cutting times and the more the system gets into the steady state.

As further material load, the plastic strain ϵ affects the flow stress. The comparison of the volume-averaged plastic strain, Fig. 13, revealed just slight differences. For the target parameter set and parameter set 1, the deviations regarding the plastic strain are not identifiable. Both, the magnitude and the local position of the volume-averaged plastic strain match each other. On the other side, small variations can be seen for the results of parameter set 2 and parameter set 3, which again are very similar. Based on the absolute differences regarding the material model parameters, the deviations regarding the local plastic strains ϵ are only small. This contributes to the assumption
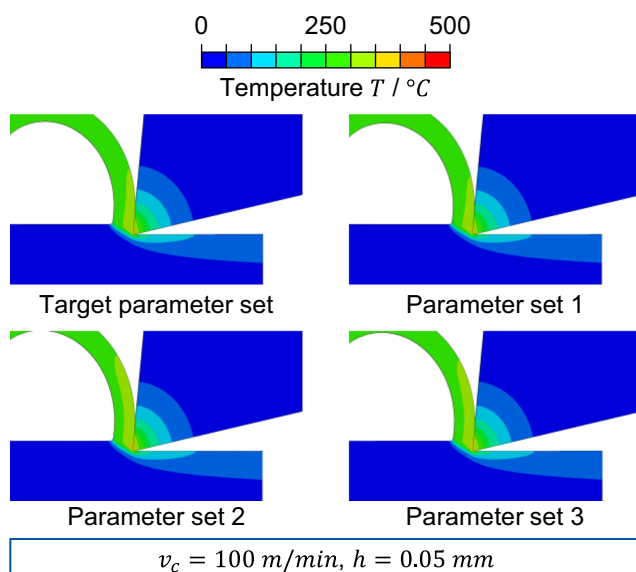

Fig. 12 Comparison of the different material model parameter sets regarding the simulated local temperatures
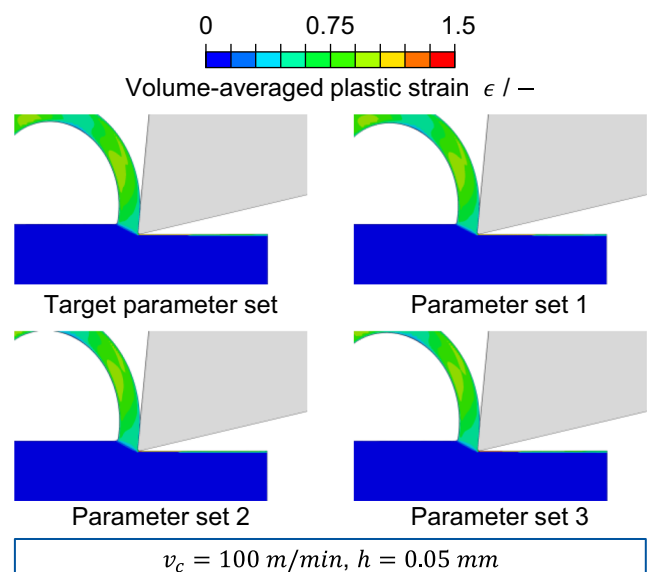

Fig. 13 Comparison of the different material model parameter sets regarding the simulated local strains
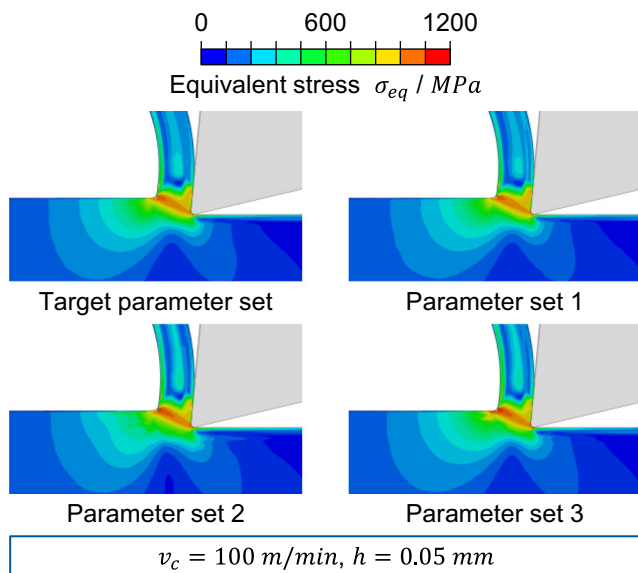
Fig. 14 Comparison of the different material model parameter sets regarding the simulated local equivalent stresses

that the considered effects of the JC model compensate each other for the investigated cutting conditions.

Figure 14 shows the equivalent stress σ_{eq} in and around the shear zone. In contrast to the comparisons of the temperature and the strain fields, the images from the simulations in Fig. 14 zoom into the cutting zone in order to enable a comparison of the local, highly resolved stress fields for the different parameter sets. As before, the equivalent stresses did not differ noticeable between the target parameter set and parameter set 1. On the other hand, small deviations can be identified for parameter set 2 and parameter set 3, which are expected to cause the differences in the considered process observables. A better agreement regarding the local stress fields is presumed for smaller error values.

The comparison of the simulation results showed that the different material parameter sets can all accurately model the locally resolved material loads. This emphasizes that uniqueness of material model parameters is no requirement to model the chip formation process within the domain of investigation of this study.

8 Summary, conclusion, and outlook

Within this paper, a novel approach to automatize the evaluation of chip formation simulations was developed. The methodology covers the determination of the chip form parameters chip thickness and chip radius from CEL chip formation simulations. The calculation of the chip form parameters proved a high accuracy. Additional procedures to average the force signal within the steady state and to compute local temperature information were established and integrated into an inverse procedure to determine material model parameters.

In the second part of the paper, the uniqueness of material model parameters for machining simulations was investigated. For this, an inverse re-identification by means of an optimization algorithm (Downhill simplex) was used on the automatized analysis of simulation results. In combination, they enable an automatic, inverse calibration of material model parameters from FE-cutting simulations. It was shown that different parameter sets can result in almost identical temperature, strain, and stress profiles. Based on the numerical results of this paper, the hypothesis of a unique set of JC material model parameters for the domain of cutting conditions cannot be supported. This was reinforced by the evaluated material loads.

The relevant findings are:

- The identification is sensitive to the initial parameter set (simplex) but manages to converge to an accurate solution in all considered cases.
- In spite of considering five process observables, the identification remains non-unique. This was attributed to the search space, which exhibits multiple local minima.
- The differences in the sets affect all effects modeled by the JC material model: strain hardening, strain rate hardening, and thermal softening and thus may compensate each other.
- The uniqueness of material model parameters is no requirement to model the chip formation process within the domain of investigation of this study.
- The non-uniqueness of the JC material model may be considered as an inherent drawback.

Based on the results of this study, the need for further research activities was identified. Firstly, the proposed methodology needs to be applied to other material models than the JC model in order to investigate the generic nature of the methodology. In this study, the JC material model was chosen due its wide applicability to model the material behavior under metal cutting conditions. However, in the state of the art, limitations for the JC model were identified, which led to the development of new material models [46]. Secondly, the automatized evaluation of the chip form was limited to the continuous chip formation under the assumption of an isotropic material. However, materials that tend to the formation of continuous chips represent only a fraction of the machined materials in industry. To extend the methodology of the inverse parameter determination to materials that tend to segmented chip formation, the automatized evaluation needs to be enhanced and the inverse routine needs to be expanded to take the parameters of a damage model into account. For anisotropic materials, a separate calibration of the material model parameters for each phase will be necessary [47]. In future studies, the methodology will be applied to experimental data in order to determine the material models and to evaluate the accuracy of a material model to describe the material behavior

under metal cutting conditions for more complex machining operations such as turning or drilling.

Author contribution MH and TB conceived this research and designed experiments; MH performed experiments and analysis; MH and TB wrote the paper and participated in the revisions of it. All authors read and approved the final manuscript.

Data availability Due to ongoing studies, the data associated with the publication are currently not available.

Code availability Due to ongoing studies, the code associated with the publication is currently not available.

Declarations

Conflict of interest The authors declare that they have no potential conflict of interest in relation to the study in this paper.

References

1. Guo Y, Wen Q (2005) A hybrid modeling approach to investigate chip morphology transition with the stagnation effect by cutting edge geometry. Trans NAMRI/SME 33:469–475

2. Lei S, Shin Y, Incropera F (1999) Thermo-mechanical modeling of orthogonal machining process by finite element analysis. Int J Mach Tools Manuf 39(5):731–750. https://doi.org/10.1016/S0890-6955(98)00059-5

3. Arrazola P, Kortabarria A, Madariaga A, Esnaola J, Fernandez E, Cappellini C, Ulutan D, Özel T (2014) On the machining induced residual stresses in IN718 nickel-based alloy. Experiments and predictions with finite element simulation. Simul Model Pract Theory 41:87–103. https://doi.org/10.1016/j.simpat.2013.11.009

4. Shi J, Liu C (2004) The influence of material models on finite element simulation of machining. J Manuf Sci Eng 126(4):849–857. https://doi.org/10.1115/1.1813473

5. Childs T (1998) Material property needs in modeling metal machining. Mach Sci Technol 2(2):303–316. https://doi.org/10.1080/10940349808945673

6. Daoud M, Jomaa W, Chatelain J, Bouzid A, Songmene V (2014) Identification of material constitutive law constants using machining tests. A response surface methodology based approach. In: de Wilde W, Hernández S, Brebbia C (eds) High performance and optimum design structure and materials. Ostend, Belgium, 09.06.2014 - 11.06.2014. WIT Press, Southampton, pp 25–36

7. Jafarian F, Imaz Ciaran M, Umbrello D, Arrazola P, Filice L, Amirabadi H (2014) Finite element simulation of machining Inconel 718 alloy including microstructure changes. Int J Mech Sci 88:110–121. https://doi.org/10.1016/j.ijmecsci.2014.08.007

8. Bäker M (2015) A new method to determine material parameters from machining simulations using inverse identification. Procedia CIRP 31:399–404. https://doi.org/10.1016/j.procir.2015.04.090

9. Arrazola P, Özel T, Umbrello D, Davies M, Jawahir IS (2013) Recent advances in modelling of metal machining processes. CIRP Ann 62(2):695–718. https://doi.org/10.1016/j.cirp.2013.05.006

10. Meslin F, Hamann J (2003) The problem of constitutive equations for the modelling of chip formation: towards inverse methods. (Series: Innovative technology series) London: Sterling VA : Kogan Page. In: van Luttervelt K, Boisse P, Altan T (eds) Friction and flow stress in forming & cutting. Sterling VA, London

11. Chandrasekaran H, M'Saoubi R, Chazal H (2005) Modelling of material flow stress in chip formation process from orthogonal milling and split Hopkinson bar tests. Mach Sci Technol 9(1):131–145. https://doi.org/10.1081/MST-200051380

12. Özel T, Zeren E (2006) A methodology to determine work material flow stress and tool-chip interfacial friction properties by using analysis of machining. J Manuf Sci Eng 128(1):119–129. https://doi.org/10.1115/1.2118767

13. Melkote S, Grzesik W, Outeiro J, Rech J, Schulze V, Attia H, Arrazola P, M'Saoubi R, Saldana C (2017) Advances in material and friction data for modelling of metal machining. CIRP Ann 66(2):731–754. https://doi.org/10.1016/j.cirp.2017.05.002

14. Venuvinod P, Jin W (1996) Three-dimensional cutting force analysis based on the lower boundary of the shear zone. Part 1. Single edge oblique cutting. Int J Mach Tools Manuf 36(3):307–323. https://doi.org/10.1016/0890-6955(95)00069-0

15. Özel T, Altan T (2000) Determination of workpiece flow stress and friction at the chip–tool contact for high-speed cutting. Int J Mach Tools Manuf 40(1):133–152. https://doi.org/10.1016/S0890-6955(99)00051-6

16. Bäker M (2004) Finite element simulation of chip formation. Habilitation: Technische Universität Carolo-Wilhelmina zu Braunschweig Braunschweig, Germany

17. Shrot A, Bäker M (2011) How to identify Johnson-Cook parameters from machining simulations. In: Menary G (ed) The 14th International Conference on Material Forming. American Institute of Physics, Melville

18. Shrot A, Bäker M (2011) Inverse identification of Johnson-Cook material parameters from machining simulations. Adv Mater Res 223:277–285. https://doi.org/10.4028/www.scientific.net/AMR.223.277

19. Shrot A, Bäker M (2012) Determination of Johnson–Cook parameters from machining simulations. Comput Mater Sci 52(1):298–304. https://doi.org/10.1016/j.commatsci.2011.07.035

20. Shrot A, Bäker M (2012) A Study of Non-uniqueness During the Inverse Identification of Material Parameters. Procedia CIRP 1:72–77. https://doi.org/10.1016/j.procir.2012.04.011

21. Klocke F, Lung D, Buchkremer S, Jawahir IS (2013) From orthogonal cutting experiments towards easy-to-implement and accurate flow stress data. Mater Manuf Process 28(11):1222–1227. https://doi.org/10.1080/10426914.2013.811738

22. Klocke F, Lung D, Buchkremer S (2013) Inverse identification of the constitutive equation of Inconel 718 and AISI 1045 from FE machining simulations. Procedia CIRP 8:212–217. https://doi.org/10.1016/j.procir.2013.06.091

23. Klocke F, Döbbeler B, Peng B, Schneider S (2018) Tool-based inverse determination of material model of Direct Aged Alloy 718 for FEM cutting simulation. Procedia CIRP 77:54–57. https://doi.org/10.1016/j.procir.2018.08.211

24. Zhang D, Zhang X, Ding H (2018) Inverse identification of material plastic constitutive parameters based on the DIC determined workpiece deformation fields in orthogonal cutting. Procedia CIRP 71:134–139. https://doi.org/10.1016/j.procir.2018.05.085

25. Shrot A, Bäker M (2010) Is it possible to identify Johnson-Cook law parameters from machining simulations? Int J Mater Form 3(S1):443–446. https://doi.org/10.1007/s12289-010-0802-4

26. Barlat F, Lege D, Brem J (1991) A six-component yield function for anisotropic materials. Int J Plast 7(7):693–712. https://doi.org/10.1016/0749-6419(91)90052-Z

27. Özel T, Karpat Y (2007) Identification of constitutive material model parameters for high-strain rate metal cutting conditions using evolutionary computational algorithms. Mater Manuf Process 22(5):659–667. https://doi.org/10.1080/10426910701323631

28. Bergs T, Hardt M, Schraknepper D (2019) Inverse material model parameter identification for metal cutting simulations by optimization strategies. MM Sci J 04:3172–3178. https://doi.org/10.17973/MMSJ.2019_11_2019067

29. Bergs T, Hardt M, Schraknepper D (2020) Determination of Johnson-Cook material model parameters for AISI 1045 from orthogonal cutting tests using the Downhill-simplex algorithm. Procedia Manuf 48:541–552. https://doi.org/10.1016/j.promfg.2020.05.081

30. Hardt M, Schraknepper D, Bergs T (2021) Investigations on the application of the Downhill-simplex-algorithm to the inverse determination of material model parameters for FE-machining simulations. Simul Model Pract Theory 107:102214–102214. https://doi.org/10.1016/j.simpat.2020.102214

31. Klocke F, Lung D, Puls H (2014) Coupled Eulerian-Lagrangian modelling of high speed metal cutting processes. In: Advances in manufacturing technology. 11th International Conference High Speed Machining, 11 - 12/9 2014, Prague, Czech Republic

32. Ducobu F, Rivière-Lorphèvre E, Filippi E (2016) Application of the coupled Eulerian-Lagrangian (CEL) method to the modeling of orthogonal cutting. Eur J Mech A Solids 59:58–66. https://doi.org/10.1016/j.euromechsol.2016.03.008

33. Johnson G, Cook W (1983) A constitutive model and data for metals subjected to large strains, high strain rates and high temperatures. In: Proceedings 7th International Symposium on Ballistics, pp 541–547

34. Nakayama Y (2018) Introduction to fluid mechanics, 2nd edn. Butterworth-Heinemann, Oxford

35. Rider W, Kothe D (1998) Reconstructing volume tracking. J Comput Phys 141:112–152

36. Youngs D (1987) An interface tracking method for a 3D Eulerian hydrodynamics code. Herausgegeben von Atomic Weapons Research Establishment

37. Kothe D, Rider W, Mosso S, Brock J, Hochstein J (1996) Volume tracking of interfaces having surface tension in two and three dimensions. In: AIAA Meeting Papers on Disc, pp 1–24 https://doi.org/10.2514/6.1996-859

38. Barth T (1992) Aspects of unstructured grids and finite-volume solvers for the Euler and Navier-Stokes equations. In: Special Course on Unstructured Grid Methods for Advection Dominated Flows, AGARD Report R-787, pp 1–61

39. Brent, R. P. (1973): Algorithms for minimization without derivatives. (Series: Prentice-Hall series in automatic computation). 1st Englewood Cliffs: Prentice-Hall

40. Brent R (1971) An algorithm with guaranteed convergence for finding a zero of a function. Comput J 14(4):422–425. https://doi.org/10.1093/comjnl/14.4.422

41. Simon D, Litt J (2011) A data filter for identifying steady-state operating points in engine flight data for condition monitoring applications. J Eng Gas Turbines Power 133(071603):1–8

42. Levinson N (1946) The Wiener (Root Mean Square) Error criterion in filter design and prediction. J Math Phys 25(1-4):261–278. https://doi.org/10.1002/sapm1946251261

43. Nelder J, Mead R (1965) A simplex method for function minimization. Comput J 7(4):308–313

44. Schwenzer M, Auerbach T, Döbbeler B, Bergs T (2019) Comparative study on optimization algorithms for online identification of an instantaneous force model in milling. Int J Adv Manuf Technol 101(9-12):2249–2257. https://doi.org/10.1007/s00170-018-3109-0

45. Vural M, Caro J (2009) Experimental analysis and constitutive modeling for the newly developed 2139-T8 alloy. Mater Sci Eng A 520(1-2):56–65. https://doi.org/10.1016/j.msea.2009.05.026

46. Zerilli F, Armstrong R (1987) Dislocation-mechanics-based constitutive relations for material dynamics calculations. J Appl Phys 61(5):1816–1825. https://doi.org/10.1063/1.338024

47. Abouridouane M, Klocke F, Lung D, Adams O (2012) A new 3D multiphase FE model for micro cutting ferritic–pearlitic carbon steels. CIRP Ann 61(1):71–74. https://doi.org/10.1016/j.cirp.2012.03.075